Novel Direct Flux and Direct Torque Control of Six-Phase Induction Machine With Nearly Square Air-Gap Flux Density

Yong-Le Ai, Maarten J. Kamper, *Member, IEEE*, and Abraham D. Le Roux, *Member, IEEE*

***Abstract*—In this paper, a novel control method for a six-phase induction machine with nearly square air-gap flux density is proposed and evaluated. In this method, the stator phase windings alternately act as either flux- or torque-producing phases. In this way, the flux and the torque of the induction machine are directly controlled with no vector transformation used. Theoretical and finite-element analyses are used to calculate, among other things, the torque and the decouple control constant of the drive. The steady-state measured results of a small six-phase induction machine drive with the proposed control scheme implemented show good agreement with calculated results. The proposed control drive system is also shown to have a fast torque response.**

***Index Terms*—Direct control, finite-element (FE) analysis, flux, six-phase induction machine, torque.**

I. INTRODUCTION

THE INHERENT disadvantages of dc drives have prompted continual progress in the area of ac drives. Among ac drives, induction machine drives are widely adopted, which are classified either under volt-per-hertz control or vector control [1]–[3].

Due to the power rating increase in drives and high reliability requirements in some special applications, many researchers have focused their research on multiphase or high phase order (HPO) induction machine drives [4]–[11]. It has been shown that HPO induction machine drives possess many advantages over conventional three-phase drives. A disadvantage, however, of HPO drives is the complexity of the control algorithm; the vector control needs complex coordinate transformations and accurate flux linkage estimators.

To address this problem and based on the research work done on HPO drives, special phase current waveforms for six-phase induction machines, which make it possible to have separate field and torque (armature) windings and currents in the machine, have been proposed [12], [13]. In this paper, the control of these field and torque windings to directly control the flux and the torque of the machine without complex coordinate transformations is investigated. The implementation of the direct control technique on a two-pole six-phase induction machine drive is explained and experimentally evaluated.

Analytical, finite-element (FE), and experimental results are presented to explain the drive's operation and to demonstrate its torque performance.

II. THEORETICAL ANALYSIS

In this section, the principle of operation and the theoretical analysis of the six-phase induction machine are briefly presented.

A. Air-Gap MMFs

To have separate rotating flux (field) and torque MMFs in a six-phase induction machine, the stator phase current waveforms can be configured, as shown in Fig. 1. This shows that the stator phase current consists of trapezoidal-shaped field and torque current components, with flat-topped amplitudes of I_f and I_t, respectively. It implies that a stator phase alternately acts in time as either a flux- or a torque-producing phase. Furthermore, it can be seen from Figs. 1 and 2 that at any instant, there are always three neighboring stator phase windings that act as field windings to generate the flux in the machine; similarly, three (other) neighboring stator phase windings always act as torque windings to generate the torque of the machine. It can be easily shown from the current waveforms of Fig. 1 and the stator winding layout of Fig. 2 that the amplitude of the resultant field MMF of the three field stator phase windings (field winding) at any instant is

$$F_f = 2N_s I_f \tag{1}$$

where N_s is the number of turns in series per phase of the stator. Similarly, the resultant amplitude of the torque MMF of the three torque stator phase windings (torque winding) at any instant is

$$F_t = 2N_s I_t. \tag{2}$$

Paper IPCSD-07-043, presented at the 2006 Industry Applications Society Annual Meeting, Tampa, FL, October 8–12, and approved for publication in the IEEE TRANSACTIONS ON INDUSTRY APPLICATIONS by the Electric Machines Committee of the IEEE Industry Applications Society. Manuscript submitted for review August 15, 2006 and released for publication April 27, 2007. This work was supported by the National Research Foundation (NRF) in South Africa.

Y.-L. Ai was with the Department of Electrical and Electronic Engineering, University of Stellenbosch, Stellenbosch 7600, South Africa. He is now with the School of Electrical Engineering and Automation, Henan Polytechnic University, Jiaozuo 454000, China (e-mail: aiyongle@hpu.edu.cn).

M. J. Kamper and A. D. Le Roux are with the Department of Electrical and Electronic Engineering, University of Stellenbosch, Stellenbosch 7600, South Africa (e-mail: kamper@sun.ac.za).

Color versions of one or more of the figures in this paper are available online at http://ieeexplore.ieee.org.

Digital Object Identifier 10.1109/TIA.2007.908157

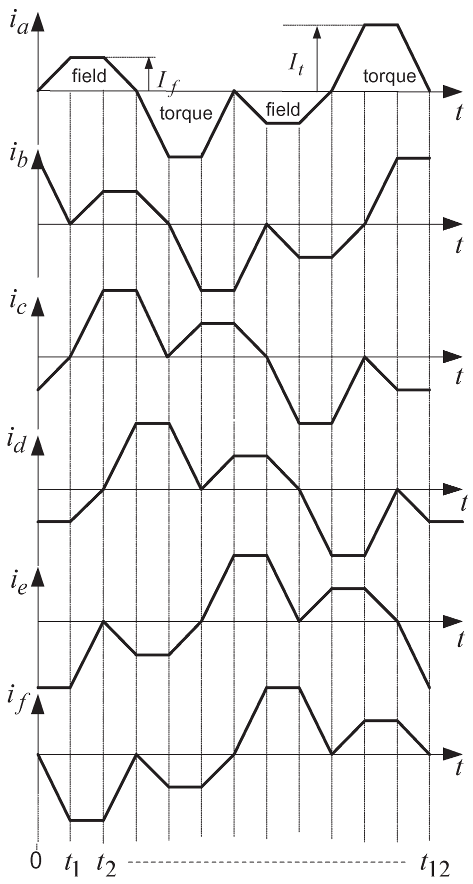

Fig. 1. Proposed six-phase stator current waveforms.

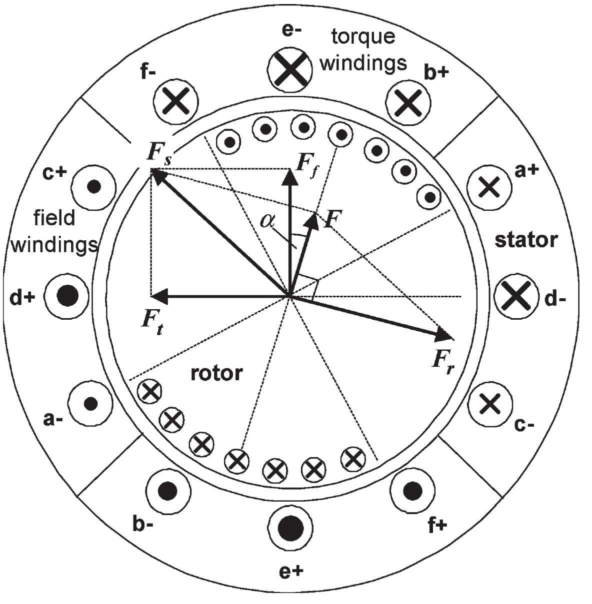

Fig. 2. Current distribution and MMF vectors at time $t = t_1/2$.

It is important to note at this stage the following.

1) The trapezoidal-shaped stator currents give rise to smooth rotating field and torque MMFs.
2) The field and torque MMFs are always perpendicular in space to each other, as shown in Fig. 2.
3) The flux-producing phase windings generate nearly square flux density in the air gap.

With nearly square air-gap flux density, square-shaped currents are induced in the rotor at a certain slip speed. Together with the two stator MMFs, there is, thus, also a rotor MMF F_r, as shown in Fig. 2. Assuming square-shaped rotor currents with 90° (electrical) conduction angle, the amplitude of the rotor MMF is given by

$$F_r = m_r N_r I_r / 2 \tag{3}$$

where m_r is the number of rotor phases (or the number of rotor bars in the case of a cage rotor), N_r is the number of turns in series per phase of the rotor (in the case of a cage rotor, $N_r = 1/2$), and I_r is the flat-top amplitude of the rotor phase or rotor bar current.

Applying vector analysis on the air-gap MMFs and noting that the resultant air-gap MMF is always perpendicular to the induced rotor MMF, as shown in Fig. 2, the amplitude of the resultant air-gap MMF is given by

$$F = \sqrt{F_s^2 - F_r^2} = \sqrt{F_f^2 + F_t^2 - F_r^2}. \tag{4}$$

From (4), the flat-topped amplitude of the air-gap flux density can be calculated by

$$B = \frac{\mu_0 F}{2\ell_g k_i} \tag{5}$$

where ℓ_g is the air-gap length, and k_i is a saturation factor that accounts for magnetic saturation in the iron teeth and yokes.

For correct operation, F_t must be amplitude controlled (by controlling I_t) in such a way that it is equal in amplitude but opposite in direction to F_r or else that $\alpha = 0$ in Fig. 2. In this way, the quadrature flux in the machine is reduced to zero to leave the original flux, which is generated by F_f and amplitude controlled by I_f, undistorted.

B. Torque Derivation

With nearly square flux density in the air gap, a nearly square electromotive force (EMF) voltage waveform is induced in the rotor phase windings or bars. The flat-topped amplitude of the rotor-induced voltage can be calculated (as for dc machines) by

$$E_r = 2N_r B l \omega_{sl} r_g \tag{6}$$

where ω_{sl} is the angular slip frequency, l is the axial stack length, r_g is the air-gap radius, and B is the air-gap flux density of (5). The flat-topped amplitude of the induced rotor phase or rotor bar current is then given by

$$I_r = \frac{E_r}{R_r} = \frac{2N_r B l \omega_{sl} r_g}{R_r} \tag{7}$$

where R_r is the rotor phase or rotor bar resistance. From this and using the Lorentz force law, the torque of the machine can be calculated by

$$T = m_r N_r B l r_g I_r. \tag{8}$$

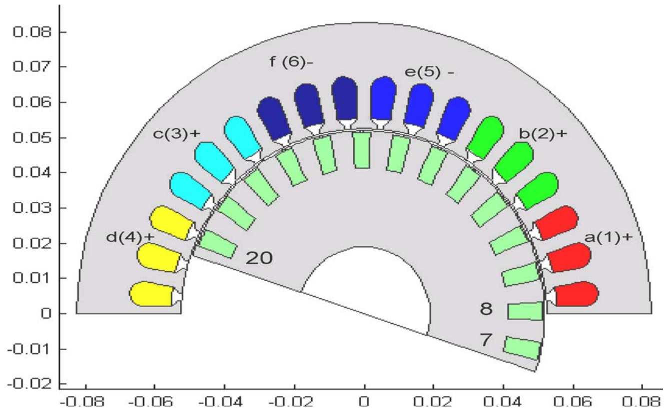

Fig. 3. Half a cross section of six-phase two-pole induction machine.

C. Balanced MMF Condition (Flux Decoupling)

For balanced MMF condition, $F_t = F_r$ and $\alpha = 0$ in Fig. 2. Hence, from (2) and (3), it follows that

$$I_t = \frac{m_r N_r I_r}{4N_s}. \tag{9}$$

From (7) and (9), the important relationship between I_t and ω_{sl} for balanced MMF control (decouple control) is obtained as follows:

$$k = \frac{\omega_{sl}}{I_t} = \left(\frac{I_r}{I_t}\right)\left(\frac{R_r}{2N_r B l r_g}\right) = \frac{2N_s R_r}{m_r N_r^2 B l r_g}. \tag{10}$$

The control gain k is, thus, dependent on two variables, namely, R_r, which is temperature sensitive, and B, which is dependent on the field current I_f. The field current can be controlled to keep B at the desired value; however, R_r can easily vary by 50% due to temperature changes. The k value used in the control system of the drive, thus, can be easily incorrect, which will disturb the MMF balance in the machine.

D. Impact of Incorrect k Value

The induction machine considered in the analysis and used in the measurements is a small two-pole induction machine of which half a cross section is shown in Fig. 3. The design data of the machine are given in Table I. The machine was originally a normal three-phase four-pole machine, which has been modified to a six-phase two-pole machine. The yoke heights are, therefore, relatively small, which requires a relatively high field current due to saturation to produce reasonable flux in the air gap. The machine has six stator phases and 14 wound rotor phases of which two phases are connected to slip rings for measurements. Using the machine data and a rated slip angular frequency of $\omega_{sl} = 15.7$ rad/s (150 r/min) and rated air-gap flux density of $B = 0.445$ T (from Section III), from (7)–(10), it can be calculated at rated condition and with MMF balance that $I_r = 5.73$ A, $I_t = 2.26$ A, $T = 6.3$ N $\cdot$ m, and $k = 6.96$ rad/(A $\cdot$ s). Thus, a typical value of $k = 7$ rad/(A $\cdot$ s) must be used in the drive control system to have decouple control.

To study the impact of an incorrect k value in the control software of the drive on the flux and the torque of the machine of Fig. 3, the machine equations in the previous sections are used as follows: first, from (3)–(5) and (7), the rotor MMF can be expressed as

TABLE I
DESIGN DATA OF INDUCTION MACHINE OF FIG. 3

Number of phases	6
Number of poles	2
Number of stator slots	36
Number of slots per pole per phase	3
Number of turns in series per stator phase, N_s	249
Stator phase resistance (Ω)	9.6
Stack outer diameter (mm)	165
Stack length, l (mm)	128
Air gap radius, r_g (mm)	49
Number of rotor slots	28
Number of rotor phases, m_r	14
Number of turns in series per rotor phase, N_r	28
Rotor phase resistance, R_r (Ω)	0.43

$$F_r = \sqrt{\frac{C^2 \omega_{sl}^2 F_s^2}{1 + C^2 \omega_{sl}^2}} \tag{11}$$

where C is given by

$$C = \frac{\mu_0 m_r N_r^2 l r_g}{2\ell_g k_i R_r}. \tag{12}$$

The flux and the torque of the machine are controlled by the currents I_f and I_t, respectively. With these currents known, the MMF amplitudes F_f, F_t, and F_s can be calculated from (1), (2), and Fig. 2. Using k as a parameter in the calculations, the slip frequency can be calculated from (10) as $\omega_{sl} = kI_t$. From this and from the known design data of the machine, I_r and F_r can be calculated according to (11) and (3), respectively. Hence, F, B, and T can be calculated according to (4), (5), and (8), respectively.

The calculated results of torque T and flux density B versus torque current I_t of the machine of Fig. 3 with k as a parameter are shown in Figs. 4 and 5. With $k = 7$, decouple control is obtained, with a linear relationship between T and I_t, and B and flux in the machine constant and independent of I_t. However, with $k \neq 7$, decouple control is lost, with the flux of the machine no longer constant and the torque a nonlinear function of I_t. In this case, due to the MMF imbalance, the angle α in Fig. 2 and the quadrature flux in the machine are no longer zero; the stator field windings in this case no longer act as flux-producing windings only but also start to act as torque windings; similarly, the stator torque and rotor windings no longer act as torque windings only but also start to act as flux-producing windings.

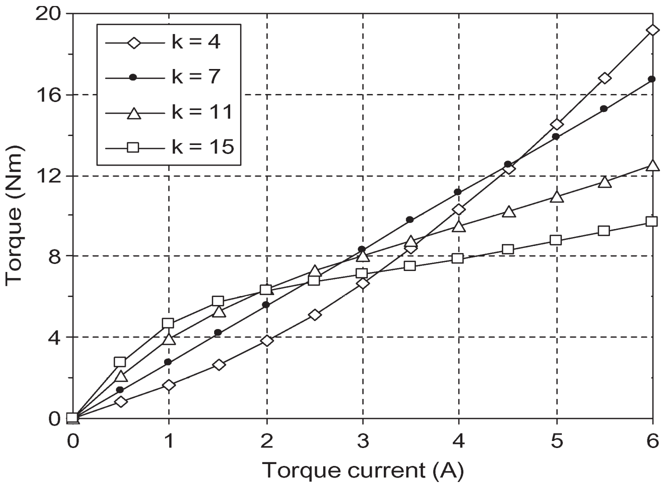

Fig. 4. Calculated impact of k on torque versus torque current of six-phase induction machine $[I_{t(\text{rated})} = 2.26\ \text{A}]$.

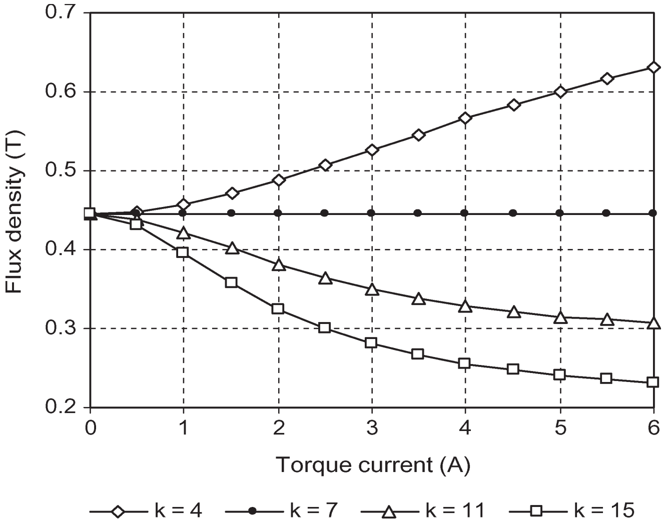

Fig. 5. Calculated impact of k on air-gap flux density versus torque current of six-phase induction machine $[I_{t(\text{rated})} = 2.26\ \text{A}]$.

III. FE Analysis

In this section, the operation of the six-phase induction machine of Fig. 3 with the phase currents of Fig. 1 under no-load and load conditions is investigated through FE analysis. Particular attention is paid in the analysis to the rotating air-gap flux, induced rotor voltage, and balanced MMF condition.

A. Air-Gap Flux Density

With only field current active, i.e., with $I_t = I_r = 0$ (no load), the radial component of the flux density in the air gap of the induction machine of Fig. 3 is determined by 2-D FE calculation. The values for the field phase currents in the FE calculation are chosen from Fig. 1 at time $t = t_1/2$, i.e., $i_a = -i_c = I_f/2$ and $i_d = -I_f$ with $I_f = 3.5$ A; the other phase currents are zero as $I_t = 0$. The effect of skew is taken into account in the 2-D FE solution by using a set of unskewed machines of which the rotors are displaced by an angle that is a fraction of the total skew; the rotor of Fig. 3 is skewed by one stator slot pitch. The result of the air-gap flux density calculation is shown in Fig. 6. The average trend of the radial component of the air-gap flux density shows a quasi-square waveform with a flat-topped amplitude of B; this is the B value used in (5)–(8) and (10).

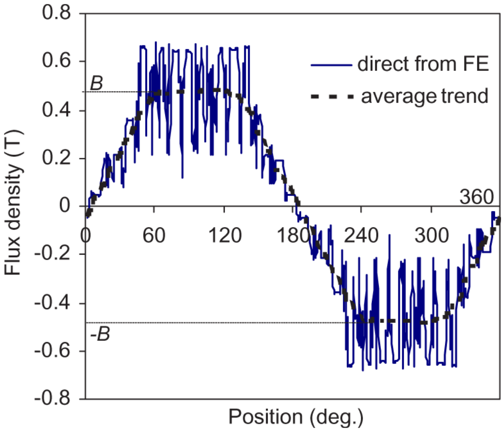

Fig. 6. Flux density distribution in air gap with skewed rotor.

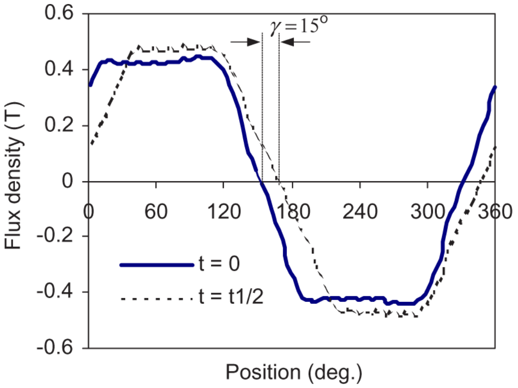

Fig. 7. Averaged air-gap flux density at different times and currents.

In Fig. 7, the average radial component of the air-gap flux density is shown at different times and different phase current values of the currents in Fig. 1. At time $t = 0$, the field phase currents are $i_c = i_d = -I_f$, whereas at time $t = t_1/2$, the currents are, again, as given above. It is clear that the flux density wave synchronously moves (rotates) with change in the phase current; however, the flat-topped amplitude B slightly varies with angular position between 0.43 and 0.46 T. This is clearer from Fig. 8, where the amplitude B is plotted versus the angular position of the flux density wave. This shows that there is a ripple in B of frequency $12f_1$, where f_1 is the fundamental frequency of the phase current. This will induce a high-frequency voltage in the rotor phase windings, which is discussed in Section III-B.

B. Rotor-Phase-Induced Voltage

To investigate the waveform of the induced voltage in a rotor phase winding of the induction machine of Fig. 3, the open-circuit voltage equation of the jth rotor phase winding, i.e.,

$$e_j = \frac{d\lambda_j}{dt} \tag{13}$$

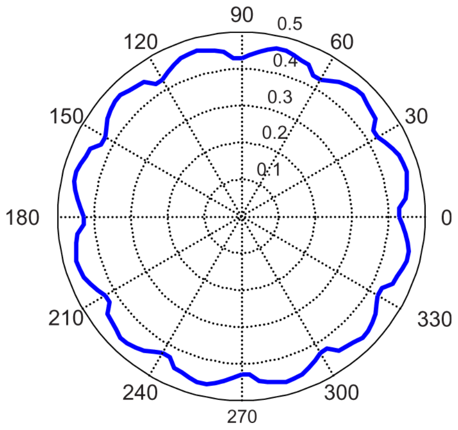

Fig. 8. Amplitude versus angular position of air-gap flux density wave.

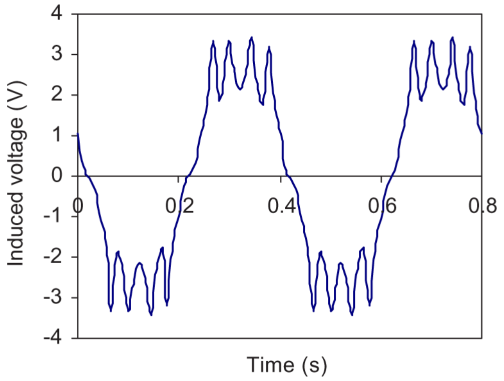

Fig. 9. Rotor-phase-induced voltage waveform with rotor at standstill.

is solved by time-stepping FE analysis. In (13), λ_j is the total flux linkage of rotor phase winding j and is calculated for the skewed rotor by

$$\lambda_j = \frac{1}{k_s} \sum_{n=1}^{k_s} \lambda_{jn}(\alpha_n) \tag{14}$$

where λ_{jn} is the flux linkage of rotor phase winding j with unskewed rotor n at position α_n, and k_s is the number of unskewed rotors. In the first investigation, the rotor is kept at standstill, and the stator field is rotated by changing the six-phase stator currents according to the waveforms of Fig. 1 with $I_f = 3.5$ A and $I_t = 0$ A. To solve for the voltage of (13), the forward difference approximation is used as

$$e_j = \frac{d\lambda_j}{dt} \approx \frac{\lambda_j(t_0 + \Delta t) - \lambda_j(t_0)}{\Delta t}. \tag{15}$$

Fig. 9 shows the FE-calculated induced rotor phase voltage at a stator field rotating speed of 150 r/min (rated slip speed). The nearly square shape of the induced voltage waveform is clear. Also, the expected $12f_1$ high-frequency component of the voltage is clear, as explained in the previous section.

In the second time-stepping FE calculations, the stator field is kept stationary, and the rotor is rotated at a speed of 150 r/min. The stator phases are supplied with phase currents $i_a = -i_c = I_f/2$, $i_d = -I_f$, and $i_b = i_e = I_f = 0$. Due to the dc stator phase currents, (13) is solved by

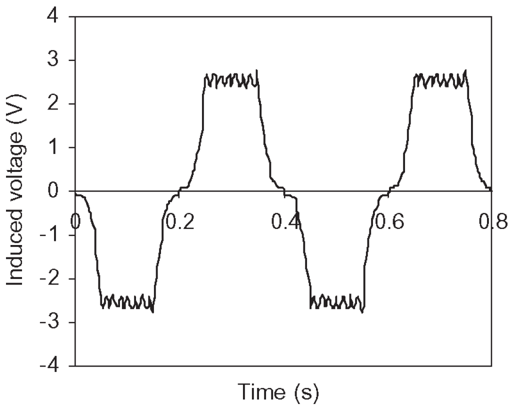

Fig. 10. Rotor-phase-induced voltage with stator field stationary and rotor rotating at 150 r/min.

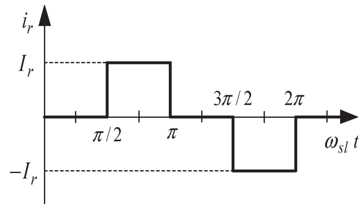

Fig. 11. Assumed rotor phase current waveform.

$$\begin{aligned} e_j &= \frac{\partial \lambda_j}{\partial i_a}\frac{di_a}{dt} + \frac{\partial \lambda_j}{\partial i_b}\frac{di_b}{dt} + \cdots + \frac{\partial \lambda_j}{\partial i_f}\frac{di_f}{dt} + \frac{\partial \lambda_j}{\partial \theta}\frac{d\theta}{dt} \\ &= \frac{\partial \lambda_j}{\partial \theta}\frac{d\theta}{dt} \approx \frac{\lambda_j(\theta + \Delta\theta) - \lambda_j(\theta)}{\Delta\theta}\omega_r \end{aligned} \tag{16}$$

using the forward difference approximation again. The result of the FE-calculated induced rotor phase voltage at a speed of 150 r/min is shown in Fig. 10. Again, the nearly square-shape waveform is evident and, in this case, very similar to the induced voltage of brushless dc machines. With the stator rotating field stationary, there is, as expected, no high ripple-induced voltage as in Fig. 9. The small ripple voltage that is visible in the waveform is due to slotting effects, both of which, in this case, are very much reduced by the skewed rotor.

C. Zero Quadrature Flux Condition

It is important to confirm the calculation of the control gain k according to (10) or, more specifically, the I_r/I_t current ratio according to (9). This can be done by looking at the resultant flux linkages of the active rotor phase windings and the torque-producing stator phase windings. For MMF balance, the quadrature flux in the machine should be zero; thus, the resultant flux linkages of these two sets of windings should be zero.

In the FE calculation of the flux linkages, it is assumed that the induced rotor phase current waveform takes up the ideal form shown in Fig. 11. This implies that dc current is

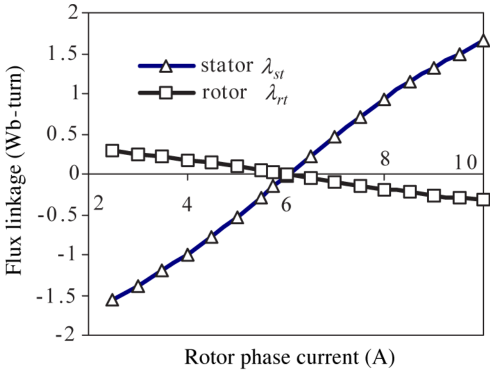

Fig. 12. Resultant flux linkage versus rotor current I_r with $I_t = 2.2$ A.

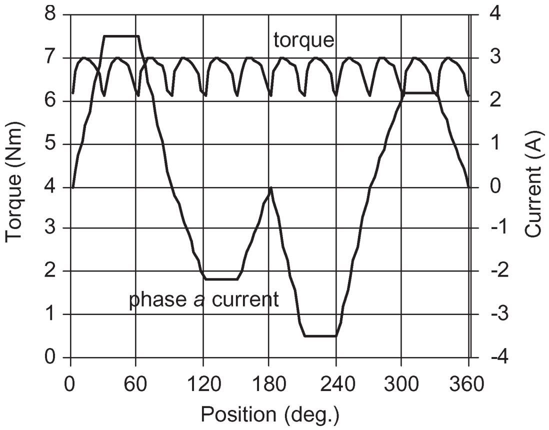

Fig. 13. FE-calculated torque of six-phase induction machine.

always flowing in 7 of the 14 rotor phases of the machine in Fig. 3. The position of the seven active rotor phase windings must be opposite to the position of the torque phase windings of the stator. In the FE analysis, rotor phase windings 11–17 and torque stator phase windings b, e, and f, as shown in Fig. 3, are made active. With these phase windings active, it is clear that the quadrature flux and the quadrature flux linkage will be in the direction of the magnetic axis of rotor phase winding 14 and stator phase winding e. Hence, the resultant flux linkage of the torque-producing stator winding set is calculated by

$$\lambda_{st} = -\lambda_b \cos\beta + \lambda_e + \lambda_f \cos\beta \tag{17}$$

where β is the angle of displacement of the stator phase windings, whereas the resultant flux linkage of the active rotor set of phase windings is calculated by

$$\begin{aligned}\lambda_{rt} = {} & \lambda_{11}\cos(3\alpha) + \lambda_{12}\cos(2\alpha) + \lambda_{13}\cos\alpha + \lambda_{14} \\ & + \lambda_{15}\cos\alpha + \lambda_{16}\cos(2\alpha) + \lambda_{17}\cos(3\alpha)\end{aligned} \tag{18}$$

where α is the angle of displacement of the rotor phase windings. The phase flux linkages in (17) and (18) are calculated by (14) for the skewed machine. In the FE calculation, the torque current I_t is kept constant at $I_t = 2.2$ A, whereas the rotor current I_r is varied to investigate the change in λ_{st} and λ_{rt}. The result of the FE flux linkage calculation is shown in Fig. 12, where a zero flux linkage condition is obtained at a rotor current of $I_r = 5.8$ A. This gives an FE-calculated current ratio for MMF balance of $I_r/I_t = 5.8/2.2 = 2.63$ compared to the theoretical calculated value according to (9) of 2.54. These values differ by less than 4%, which confirms the theoretical calculation of the gain k according to (9) and (10).

D. FE Torque Calculation

The torque of the six-phase induction machine is also directly calculated from the FE solution. As in (14), the skewed torque is calculated by using k_s unskewed machines as

$$T = \frac{1}{k_s}\sum_{n=1}^{k_s} T_i \tag{19}$$

where T_i is the torque of the ith unskewed machine determined by the Maxwell stress tensor method. Through time-stepping FE analysis, the torque of the machine in Fig. 3 is calculated according to (19) at rated and balanced MMF conditions, i.e., with $I_f = 3.5$ A, $I_t = 2.2$ A, and $I_r = 5.6$ A at a rated slip speed. Note that in this calculation, dc current is assumed in seven of the rotor phases with the rotor synchronously rotating with the stator field. The result of this calculation is shown in Fig. 13, where the $12f_1$ ripple frequency in the torque due to the phase current waveforms is evident.

IV. MEASURED AND CALCULATED RESULTS

In this section, the six-phase induction machine drive used in the testing is described followed by the presentation of measured and calculated results of induced voltage, air-gap flux density, torque, dynamic performance, and rotor-induced current.

A. Description of Drive

A block diagram of the six-phase induction machine drive and its control is shown in Fig. 14. A full bridge inverter is necessary for each stator phase winding, which results in 12 phase legs. For this, four PS21867 three-phase power inverter modules are used to complete the six-phase full bridge inverter. The six-phase induction machine, built in a standard 2.2-kW induction machine frame, is mechanically connected to a dc machine as load via a torque sensor.

The rotor position and six phase currents of the drive are measured and fed back to the floating point TMS320VC33 DSP controller, as shown in Fig. 14. The speed controller controls the torque command current I_t from which the slip angular frequency ω_{sl} is determined using the important control gain k of (10). From this and from the known field command current I_f, the six reference phase currents of the drive are generated. A digitally implemented hysteresis current regulator, using, among others, a field-programmable gate array, is used for the current control. The switching signals are sent to the inverter via fiber-optic cables.

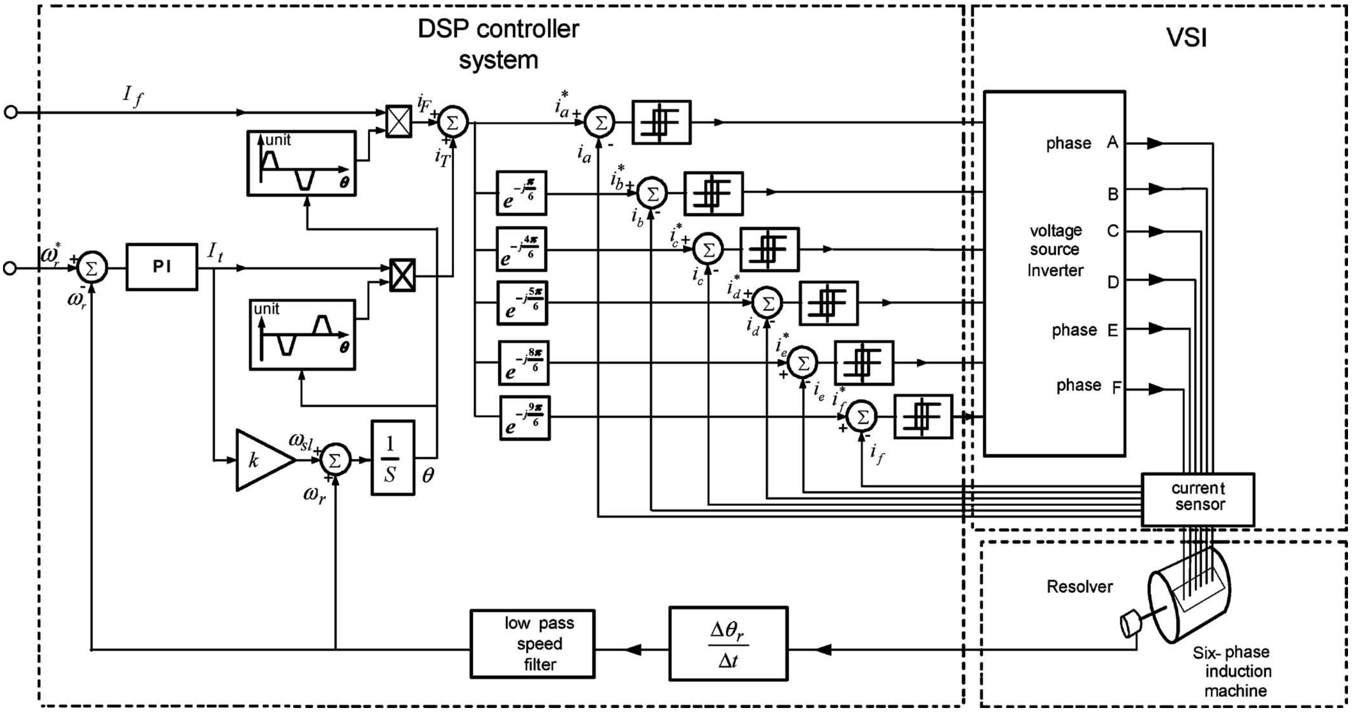

Fig. 14. Block diagram of six-phase induction machine drive.

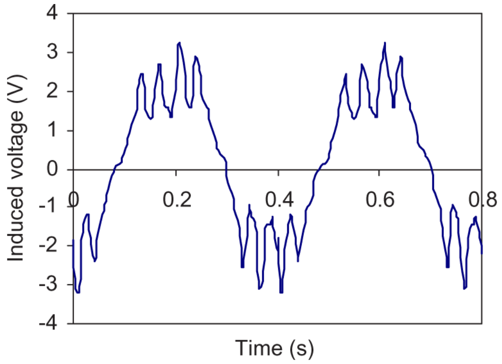

Fig. 15. Measured open-circuit rotor-induced voltage waveform with rotor at standstill.

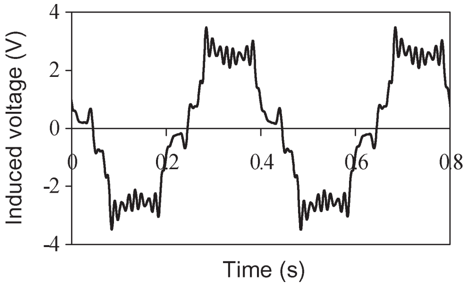

Fig. 16. Measured open-circuit rotor-induced voltage waveform with stator field at standstill.

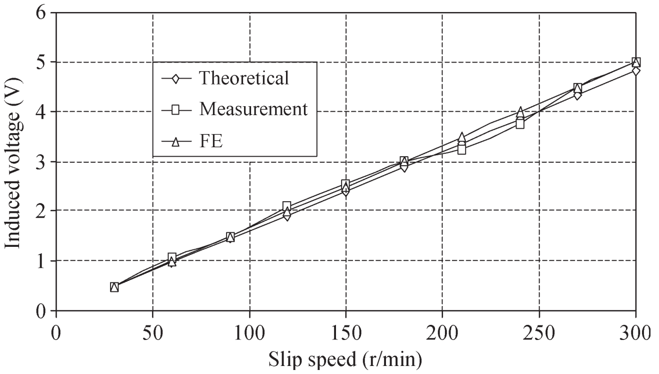

Fig. 17. Induced rotor voltage amplitude E_r versus slip speed ($I_f = 3.5$ A).

B. Rotor-Phase-Induced Voltage

The open-circuit induced rotor phase voltage is measured with the rotor at standstill and the stator field rotating at a rated slip speed (150 r/min), and vice versa. The measured results for these two conditions are shown in Figs. 15 and 16 and confirm the time-stepping FE-calculated results of Figs. 9 and 10, respectively, under the same conditions. In Fig. 17, with constant field current, the measured average induced flat-topped amplitude voltage E_r versus slip speed is compared with the theoretical and average FE-calculated amplitude voltage. This shows excellent agreement and also shows the expected linear relationship between voltage and slip speed.

C. Air-Gap Flux Density Evaluation

The flat-topped amplitude of the air-gap flux density B can be measured by using (6) and measuring E_r and ω_{sl}. The measurement of B in this way versus field current I_f is shown and compared with FE calculations in Fig. 18. Fairly good agreement is obtained between measured and FE-calculated results; the FE calculation obviously depends on the saturated B–H curve of the steel used in the analysis. Also clear from this

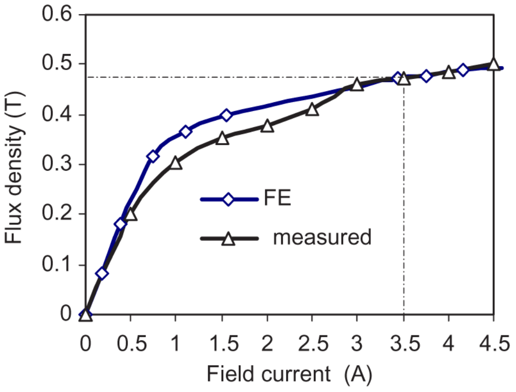

Fig. 18. Comparison of air-gap flux density.

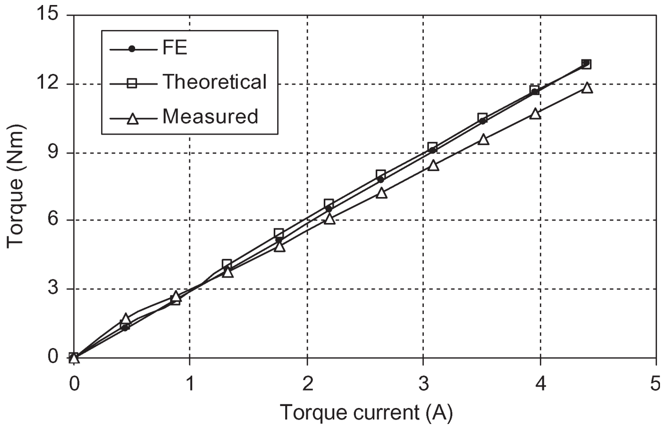

Fig. 19. Torque versus torque current I_t at rated field current and locked rotor $(I_{t(\text{rated})} = 2.26\ \text{A})$.

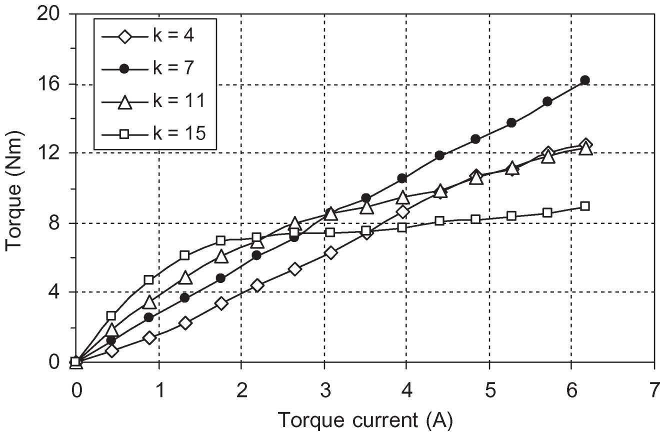

Fig. 20. Measured torque versus torque current I_t at rated field current and locked rotor and k as a parameter $[I_{t(\text{rated})} = 2.26\ \text{A}]$.

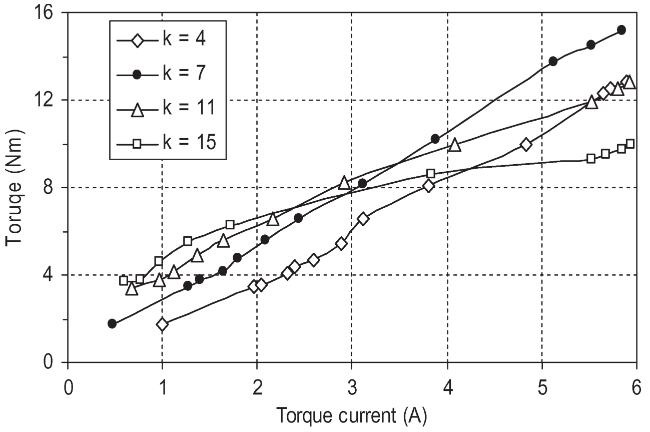

Fig. 21. Measured torque versus torque current I_t at rated field current and 800 r/min and k as a parameter $(I_{t(\text{rated})} = 2.26\ \text{A})$.

figure is the relatively high field current of $I_f = 4.5$ A, which is required to obtain a flux density of 0.5 T in the air gap.

D. Torque Evaluation

The torque of the six-phase induction machine drive is measured under locked-rotor and rotating-rotor conditions. In both cases, the field current is kept constant at $I_f = 3.5$ A. The latter corresponds to a B value from the FE analysis of 0.45 T; this value is used in the theoretical torque calculation according to (8). The FE-calculated torque is determined by averaging the torque calculated according to (19).

The measured and calculated torque results versus torque current with the rotor locked are shown in Fig. 19. Good agreement is shown between theoretical and FE calculations; however, a 9% lower torque is measured. The reason for the latter is that the waveform of the induced rotor phase current deviates from the waveform assumed in the analysis (Fig. 11).

Another important result from Fig. 19 is the measured linear relationship between the torque and the torque current of the drive. This is very important as it shows that the MMF balance or the zero quadrature flux is maintained in the machine by the drive controller, independent of the load current.

To investigate the impact of an incorrect k value of (10) on the torque performance of the drive, the torque versus torque current of the drive is measured for different k values used in the control system of Fig. 14. A locked-rotor test, as well as a rotating-rotor test, was conducted. For the rotating-rotor test, the speed of the drive is adjusted to 800 r/min and was kept constant at this speed by means of the speed controller. The results of the measurements are shown in Figs. 20 and 21. The rotating test was difficult to carry out with the speed controller active (specifically with $k = 15$); this explains the uneven curves of Fig. 21 and the slight difference between the results of Figs. 20 and 21. Nevertheless, it is clear from these figures that with $k = 7$, decouple control is obtained, with the generated torque a linear function of torque current up to 2.7 per unit load. The relatively good agreement between the measured results of Fig. 20 and the calculated results of Fig. 4 is remarkable considering the simple theoretical analysis used. The biggest difference is with $k = 4$; however, this is due to the linear magnetic circuit assumed in the calculations. The air-gap flux density will not increase as far due to saturation, as theoretically predicted in Fig. 5 with $k = 4$.

E. Dynamic Performance

The six-phase induction machine drive was also tested for its dynamic performance. In Fig. 22, the measured torque and the stator phase current response of the drive for step input torque current commands are shown (all measurements were

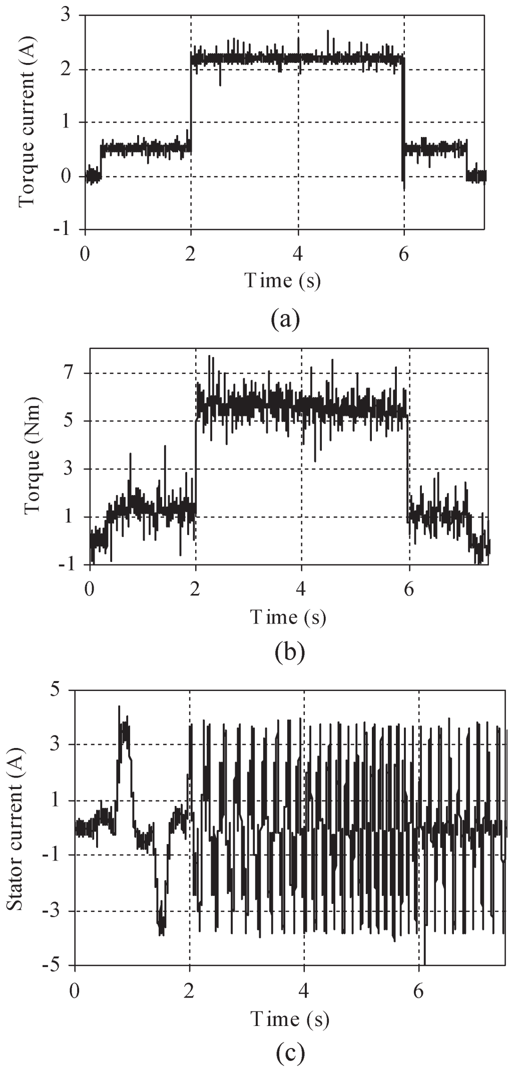

Fig. 22. Measured torque and current response to step input torque current command. (a) Command torque current. (b) Torque. (c) Stator phase current.

done with a digital oscilloscope). This shows that the fast torque response of the drive is obtained. The slight decrease in the measured torque as speed increases is due to the viscous friction loss torque of the induction machine with its slip rings. Fig. 23 shows the speed and the torque current response of the drive for a step input speed command. The long speedup time is due to the large inertia of the system and the limiting of the torque current to 4.5 A.

F. Rotor Phase Current

The induced rotor phase current is measured with the rotor locked and the stator field rotating at a rated slip speed and control gain $k = 7$. The measured stator and rotor phase current waveforms under these conditions are shown in Fig. 24. It is clear that the rotor current waveform has a quasi-square shape with a flat amplitude. However, it substantially deviates from the assumed waveform of Fig. 11. The average of the flat-topped amplitude of the rotor current is measured as 6.7 A, which is higher than the calculated rotor current amplitude of $I_r = 5.7$ A given earlier.

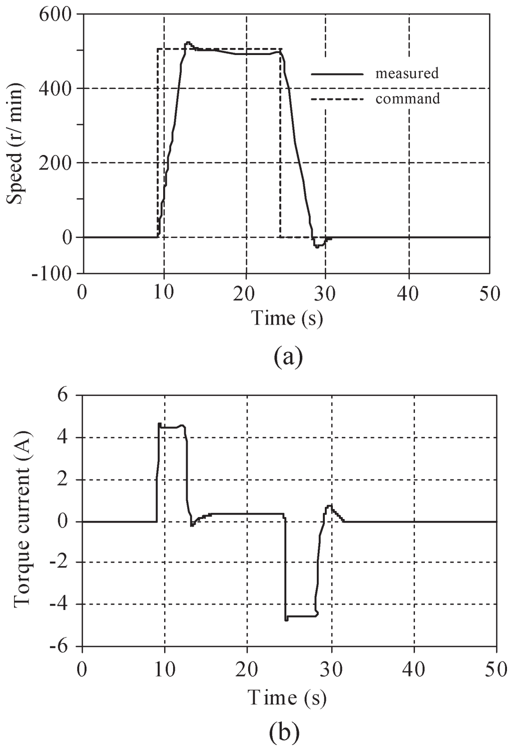

Fig. 23. Measured (filtered) (a) speed and (b) stator torque current for step input speed command.

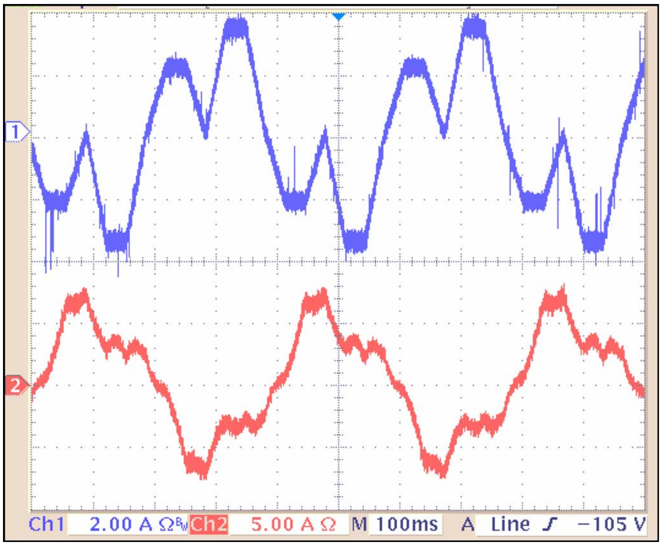

Fig. 24. Measured stator (Ch1) and rotor (Ch2) current waveforms at locked rotor and rated slip frequency (2.5 Hz) and $k = 7$ ($I_t = 2.2$ A; $I_f = 3.5$ A).

V. CONCLUSION

A new control method for six-phase induction machine drives, whereby flux and torque are directly controlled by means of field and torque currents and windings, was proposed and successfully implemented. It is a very simple direct control scheme, which is not only limited to six-phase machine drives but can be also used for any HPO drive. With this control method, the ease of the torque performance calculations is conspicuous. From the investigation, the following conclusions are reached.

1) The calculated results from simple theoretically derived formulas for the proposed drive are in good agreement with FE-calculated and measured results. This is particularly the case for the formula of the MMF balance (decoupling) constant used in the control software.
2) The proposed phase current waveforms generate nearly square-shape smooth rotating flux density in the air gap. The smooth rotating flux is important for proper induction machine operation.
3) The proposed phase current waveforms give rise to a $12f_1$ ripple frequency in the flat-topped amplitude of the back EMF. The possible negative effect of this on efficiency and ripple torque of the drive must be further investigated.
4) The measured linear relationship between torque and torque current of the drive shows that the MMF balance and the flux decoupling are maintained in the machine by the drive controller independent of the load condition. This implies that separate and direct control of the torque is obtained as in brush and permanent magnet brushless dc machine drives.
5) Instead of the expected square-shape rotor current waveform, a trapezoidal-shaped waveform is measured. Aspects of the exact rotor current waveform and the utilization of the rotor windings must be further investigated.

REFERENCES

[1] B. K. Bose, *Modern Power Electronics and AC Drives*. Englewood Cliffs, NJ: Prentice-Hall, 2002.

[2] P. Vas, *Vector Control of AC Machines*. Oxford, U.K.: Oxford Sci., 1990.

[3] D. W. Novotny and T. A. Lipo, *Vector Control and Dynamics of AC Drives*. New York: Oxford Univ. Press, 1997.

[4] E. E. Ward and H. Harea, "Preliminary investigation of an inverter fed 5-phase induction motor," *Proc. Inst. Electr. Eng.*, vol. 116, no. 6, pp. 980–984, Jun. 1969.

[5] R. H. Nelson and P. C. Krause, "Induction machine analysis for arbitrary displacement between multiple winding sets," *IEEE Trans. Power App. Syst.*, vol. PAS-93, no. 3, pp. 841–848, May 1974.

[6] E. A. Klingshirn, "High phase order induction motors—Part I: Description and theoretical consideration," *IEEE Trans. Power App. Syst.*, vol. PAS-102, no. 1, pp. 47–53, Jan. 1983.

[7] E. A. Klingshirn, "High phase order induction motors—Part II: Experimental results," *IEEE Trans. Power App. Syst.*, vol. PAS-102, no. 1, pp. 54–59, Jan. 1983.

[8] T. A. Lipo, "A d–q model for six-phase induction machine," in *Proc. ICEM*, Athens, Greece, 1980, pp. 860–867.

[9] Y. Zhao and T. A. Lipo, "Space vector PWM control of dual three-phase induction machine using vector space decomposition," *IEEE Trans. Ind. Appl.*, vol. 31, no. 5, pp. 1100–1109, Sep./Oct. 1995.

[10] H. A. Toliyat and H. Xu, "A novel direct torque control (DTC) method for five-phase induction machines," in *Proc. IEEE APEC*, 2000, vol. 1, pp. 162–168.

[11] G. K. Singh, K. Nam, and S. K. Lim, "A simple indirect field-oriented control scheme for multiphase induction machine," *IEEE Trans. Ind. Electron.*, vol. 52, no. 4, pp. 1177–1184, Aug. 2005.

[12] Y. Ai, M. J. Kamper, Y. Wang, and S. Yuan, "Torque performance investigation of double three-phase motor using special current waveform," in *Proc. 4th IPEMC Conf.*, Xian, China, Aug. 2004, pp. 1673–1678.

[13] Y. Ai, M. J. Kamper, and Y. Wang, "Investigation of airgap flux density and torque performance of six-phase induction motor with special phase current waveform," in *Proc. 8th ICEMS*, Nanjing, China, Sep. 2005, pp. 99–104.

Yong-Le Ai was born in China in 1963. He received the M.S. degree in engineering from Southwest Jiaotong University, Chengdu, China, in 1995, and the Ph.D. degree from the University of Stellenbosch, Stellenbosch, South Africa, in 2006.

He is currently a Lecturer with the School of Electrical Engineering and Automation, Henan Polytechnic University, Jiaozuo, China. His interests are in power electronics, electrical drives, and control.

Maarten J. Kamper (M'96) received the M.Sc. (Eng) and Ph.D. (Eng) degrees from the University of Stellenbosch, Stellenbosch, South Africa, in 1987 and 1996, respectively.

In 1989, he joined the academic staff of the Department of Electrical and Electronic Engineering, University of Stellenbosch, where he is currently a Professor of electrical machines and drives. His research area is computer-aided design and control of reluctance, permanent-magnet, and induction electrical machine drives.

Prof. Kamper is a South African National Research Foundation supported scientist and a Registered Professional Engineer in South Africa.

Abraham D. Le Roux (M'99) was born in Citrusdal, South Africa, in 1973. He received the B.Eng. and M.Eng. degrees in electrical engineering from the University of Stellenbosch, Stellenbosch, South Africa, in 1996 and 1998, respectively.

He is currently a part-time Lecturer with the Department of Electrical and Electronic Engineering, University of Stellenbosch. His research interests include digital controllers, digital control applied to power electronics, and active filters.